THE JOURNAL OF BIOLOGICAL CHEMISTRY VOL. 291, NO. 9, pp. 4684–4697, February 26, 2016

JMJD5 (Jumonji Domain-containing 5) Associates with Spindle Microtubules and Is Required for Proper Mitosis*[S]

Received for publication, June 18, 2015, and in revised form, December 17, 2015 Published, JBC Papers in Press, December 18, 2015, DOI 10.1074/jbc.M115.672642

Zhimin He[‡1], Junyu Wu[‡1], Xiaonan Su[‡1], Ye Zhang[‡], Lixia Pan[‡], Huimin Wei[§], Qiang Fang[§], Haitao Li[‡], Da-Liang Wang[‡2], and Fang-Lin Sun[‡§3]

From the [‡]Department of Basic Medical Sciences, School of Medicine, Tsinghua University, Beijing 100084, China and [§]Research Center for Translational Medicine at East Hospital, School of Life Sciences and Technology, Tongji University, Shanghai 200092/200120, China

Precise mitotic spindle assembly is a guarantee of proper chromosome segregation during mitosis. Chromosome instability caused by disturbed mitosis is one of the major features of various types of cancer. JMJD5 has been reported to be involved in epigenetic regulation of gene expression in the nucleus, but little is known about its function in mitotic process. Here we report the unexpected localization and function of JMJD5 in mitotic progression. JMJD5 partially accumulates on mitotic spindles during mitosis, and depletion of JMJD5 results in significant mitotic arrest, spindle assembly defects, and sustained activation of the spindle assembly checkpoint (SAC). Inactivating SAC can efficiently reverse the mitotic arrest caused by JMJD5 depletion. Moreover, JMJD5 is found to interact with tubulin proteins and associate with microtubules during mitosis. JMJD5-depleted cells show a significant reduction of α-tubulin acetylation level on mitotic spindles and fail to generate enough interkinetochore tension to satisfy the SAC. Further, JMJD5 depletion also increases the susceptibility of HeLa cells to the antimicrotubule agent. Taken together, these results suggest that JMJD5 plays an important role in regulating mitotic progression, probably by modulating the stability of spindle microtubules.

In eukaryotic cells, accurate chromosome segregation during cell division relies on the proper assembly of a bipolar spindle during mitosis. Disturbed mitosis may result in genome instability and is one of the major features of many types of cancer (1). Chromosome instability caused by abnormal mitosis is correlated with tumor grade and prognosis (2–4). Spindle assembly checkpoint (SAC)[4] is a procedure that ensures precise bipolar mitotic spindle assembly, faithful kinetochore-spindle microtubule attachment, and proper chromosome segregation (5, 6). When SAC is activated, BubR1, Mad2, and Bub3, along with Cdc20, form the mitotic checkpoint complex to prevent the anaphase-promoting complex/cyclosome from promoting cyclin B and securin degradation and mitosis exiting; these events arrest cells in metaphase (5, 7).

Post-translational modifications on microtubules are crucial for regulating microtubule properties and functions (8). Spindle microtubules, as the fundamental drivers of chromosome segregation in mitosis, are highly modified with acetylation, detyrosination, and polyglutamination. These modifications can influence the interactions of microtubules with a variety of microtubule-associated proteins (9), and the microtubule-associated proteins, conversely, can regulate the stability of spindle microtubules, such as TPX2 (10), HURP (11), and NuSAP (12).

JMJD5, also named KDM8, was reported to be responsible for gene transcription regulation through its histone H3 lysine 36 dimethylation (H3K36me2) demethylase activity (13–15) and to regulate osteoclastogenesis with its hydroxylase activity (16). It regulated cell cycle progression in breast cancer cells by CCNA1 transcription regulation (13), and proliferation of mouse embryonic cells through regulating Cdkn1a (14). Research into JMJD5 interacting partners revealed its role in metabolism by regulating PKM2 nuclear translocation (17) and in chromosome segregation along with RCCD1 (18). Additionally, JMJD5 was recently shown to be essential for maintaining the short G_1 phase in human embryonic stem cells (19). Although previous studies have shown a transcriptional regulation role of JMJD5 in cell cycle progression, the precise function of JMJD5 in mitosis is still unclear.

In this study, we found that during mitosis, JMJD5 diffused into cytoplasm and partially accumulated on spindles. Further, we showed that JMJD5 was associated with microtubules and regulated the stability of spindle microtubules. Depletion of JMJD5 led to abnormal spindle assembly and resulted in significant accumulation of mitotic cells by activating SAC. Also we found that JMJD5 depletion enhanced the cytotoxic responses of HeLa cells to nocodazole, an antimicrotubule agent. These data revealed a novel role of JMJD5 in regulating microtubule stability and mitotic progression.

Experimental Procedures

Reagents and Antibodies—Thymidine, nocodazole, taxol, and propidium iodide were purchased from Sigma-Aldrich.

* This work was supported by the National Natural Science Foundation of China Grant 91419304 and the 973 program of the Ministry of Science and Technology of China Grant 2015CB964800, 2015CB856200, 2011CB965300, 2013CB967600, and 2013CB967500. The authors declare that they have no conflicts of interest with the contents of this article.
[S] This article contains supplemental Movies S1 and S2.
[1] These authors contributed equally to this work.
[2] To whom correspondence may be addressed: Dept. of Basic Medical Sciences, School of Medicine, Tsinghua University, Beijing 100084, China. Tel.: 86-10-62792344; E-mail: wangdaliang@mail.tsinghua.edu.cn.
[3] To whom correspondence may be addressed: Research Center for Translational Medicine at East Hospital, School of Life Sciences and Technology, Tongji University, Shanghai 200092/200120, China. Tel.: 86-21-65980910; E-mail: sfl@tongji.edu.cn.
[4] The abbreviations used are: SAC, spindle assembly checkpoint; ACA, anti-centromere antibody; DTB, double thymidine block; IF, immunofluorescent.

Tubastatin A was purchased from Selleckchem. Antibodies used in this study were purchased from the indicated companies: The rabbit polyclonal antibodies were anti-JMJD5 (Millipore), anti-JMJD5 (Abmart), phosphohistone H3 (Ser10) antibody (Alexa Fluor® 488 conjugate) (Cell Signaling Technology), anti-α-tubulin (Bioworld), anti-cyclinB1 (Bioworld), anti-GFP (MBL), anti-GST (EasyBio), anti-His (EasyBio), anti-RCCD1 (Abcam), anti-MCM7 (Abgent), anti-BAG2 (Abgent), anti-CSNK1G1 (Abgent), anti-PSMD2 (Bioworld), and anti-H3.1 (Abcam). The rabbit mAb was anti-acetyl-α-tubulin (Cell Signaling Technology). The mouse monoclonal antibodies were anti-HA (Abmart), anti-GFP (Abmart), anti-GAPDH (EasyBio), anti-β-tubulin (EasyBio), anti-Histone H3 (phospho Ser10) (Abcam), anti-BubR1 (Abcam), anti-γ-tubulin (Abcam), and anti-α-tubulin (Sigma-Aldrich). Other antibodies used include human anti-centromere antibody (ACA; Antibodies Inc.; a gift from Dr. Chuanmao Zhang, Peking University), goat anti-mouse FITC and goat anti-rabbit CY3 (Jackson ImmunoReseach), and goat anti-human FITC (Beyotime).

Plasmids and siRNAs—Human JMJD5 and mouse JMJD5 cDNAs were obtained by RT-PCR from HeLa cells and R1 mESCs. JMJD5 cDNAs were cloned into pCDNA3.1-mcherry, pEGFP-N1, phGST.1 (20), pEF-Neo-Flag, and pcDNA3.1-HA vector (from Dr. Zhijie Chang, Tsinghua University, Beijing, China). To generate mJMJD5 H319A/D321A mutant, PCR-based site-directed mutagenesis was performed using Q5® high fidelity DNA polymerase (New England Biolabs) with primers 5′-CCATCTCCCCACTGGCTCAGGCCCCCCAGCAGAACTTC-3′ (forward) and 5′-GAAGTTCTGCTGGGGGGCCTGAGCCAGTGGGGAGATGG-3′ (reverse). The mutation was verified by sequencing.

Control siRNA (5′-UUCUCCGAACGUGUCACGUTT-3′), siJMJD5–2 (5′-CCAGAUGUGAAGUUAGAAATT-3′), and Mad2 SMART pool (5′-GAAAGAUGGCAGUUUGAUA-3′, 5′-UAAAUAAUGUGGUGGAACA-3′, 5′-GAAAUCCGUUCAGUGAUCA-3′, and 5′-UUACUCGAGUGCAGAAAUA-3′) (21) were synthesized by GenePharma (Shanghai, China). The siJMJD5–1 (sc-75359) and JMJD5 CRISPR/Cas9 KO Plasmid (sc-405787) were purchased from Santa Cruz Biotechnology.

Cell Culture, Transfection, and Synchronization—HeLa cells were purchased from National Platform of Experimental Cell Resources for Sci-Tech (China). The cells were maintained in DMEM supplemented with 10% FBS and 1% streptomycin/penicillin at 37 °C in a humidified atmosphere with 5% CO_2. siRNA was transfected using RNAiMAX (Life Technologies) according to the manufacturer's instructions in medium without antibiotics. The plasmids were transfected using Lipofectamine 2000 or Lipofectamine 3000 (Life Technologies).

The cells were synchronized by double thymidine block (DTB) and release or by nocodazole treatment. For DTB and release, the cells were treated with 4 mM thymidine for 17 h, released in fresh medium for 8 h, and then treated with 4 mM thymidine again for 15 h. Cells in different phases were harvested sequentially at the indicated time points after being released from DTB. To get more M phase cells, the cells were synchronized by nocodazole treatment. Briefly, the cells were treated with 4 mM thymidine for 17 h, released in fresh medium for 4 h, and then treated with 100 ng/ml nocodazole for 17 h. The cells were shaken off and extracted directly for immunoprecipitation or released back in fresh medium and harvested sequentially at the indicated time points to analyze mitotic exiting.

Immunofluorescence Microscopy—HeLa cells grown on polylysine-coated glass coverslips were fixed with methanol at −20 °C or 4% paraformaldehyde at room temperature. Then the cells were permeabilized and blocked in PBS-BT buffer (1× PBS, 3% (m/V) BSA, and 0.1% Triton X-100) at room temperature. The cells were incubated with diluted primary antibodies at 4 °C overnight and then with diluted (1:200) FITC- or CY3-conjugated secondary antibodies at room temperature in dark for 1 h. Coverslips were mounted in VECTASHIELD mounting medium with DAPI (VECTOR laboratory). The images were acquired using an A1R MP multiphoton confocal microscope (Nikon) under 100× oil objective and analyzed with NIS-Elements software (Nikon).

Flow Cytometric Analysis of Cell Mitotic Index—Cell mitotic index was evaluated as described previously with some modifications (22). Briefly, the cells were fixed with 1% paraformaldehyde followed by ice-cold 80% ethanol. The cells were then permeabilized with 0.25% Triton X-100 and incubated with diluted Alexa Fluor 488 conjugate anti-phosphohistone H3 (Ser10) antibody in dark. The cells were washed once and resuspended in PBS containing propidium iodide and RNase A (Takara) on ice for 30 min. Mitotic index was determined using BD FACSCalibur, and the data were analyzed by CellQuest™ Pro software (BD Biosciences).

CRISPR/Cas9 JMJD5 Knock-out Cell Line Generation—HeLa cells were transfected with CRISPR/Cas9 JMJD5 KO Plasmids with Lipofectamine 3000, and GFP-positive cells were selected by FACS after 24 h. Single cell colonies were selected and tested by Western blot.

Time Lapse Microscopy Imaging and Analysis of Mitotic Duration—HeLa cells stably expressing H2B-GFP were transfected with siRNAs or siRNAs together with pcDNA3.1-mcherry, mJMJD5-WT-mcherry, and mJMJD5-mut-mcherry plasmids and then synchronized by DTB and released for 6 h. Then living cell microscopy was performed on an OLYMPUS IX81-ZDC microscope with 10× objective (to get more cells for calculation). Images were taken approximately every 3 min and were analyzed with CellSens Dimension software (Olympus). The duration of mitosis was calculated according to the time lapse images from the sign of chromosome condensation at prophase to chromosome decondensation at telophase.

Gene Ontology Analysis and Protein-Protein Interaction Network Construction—Identified JMJD5 interactors were categorized into functional groups using DAVID (Database for Annotation, Visualization and Integrated Discovery) (23). The protein-protein interaction data for these proteins were retrieved from the BioGRID database (24), and a new interaction network was generated using Cytoscape software (25).

GST Pulldown Assay—GST and the JMJD5-GST fusion protein were expressed in *Escherichia coli*. BL21 (DE3) and immobilized on glutathione-Sepharose beads (GE Healthcare). The beads were washed three times with lysis buffer before incubation with whole cell lysate (cells after nocodazole synchronization and released for 30 min) at 4 °C for 2 h. Then the beads

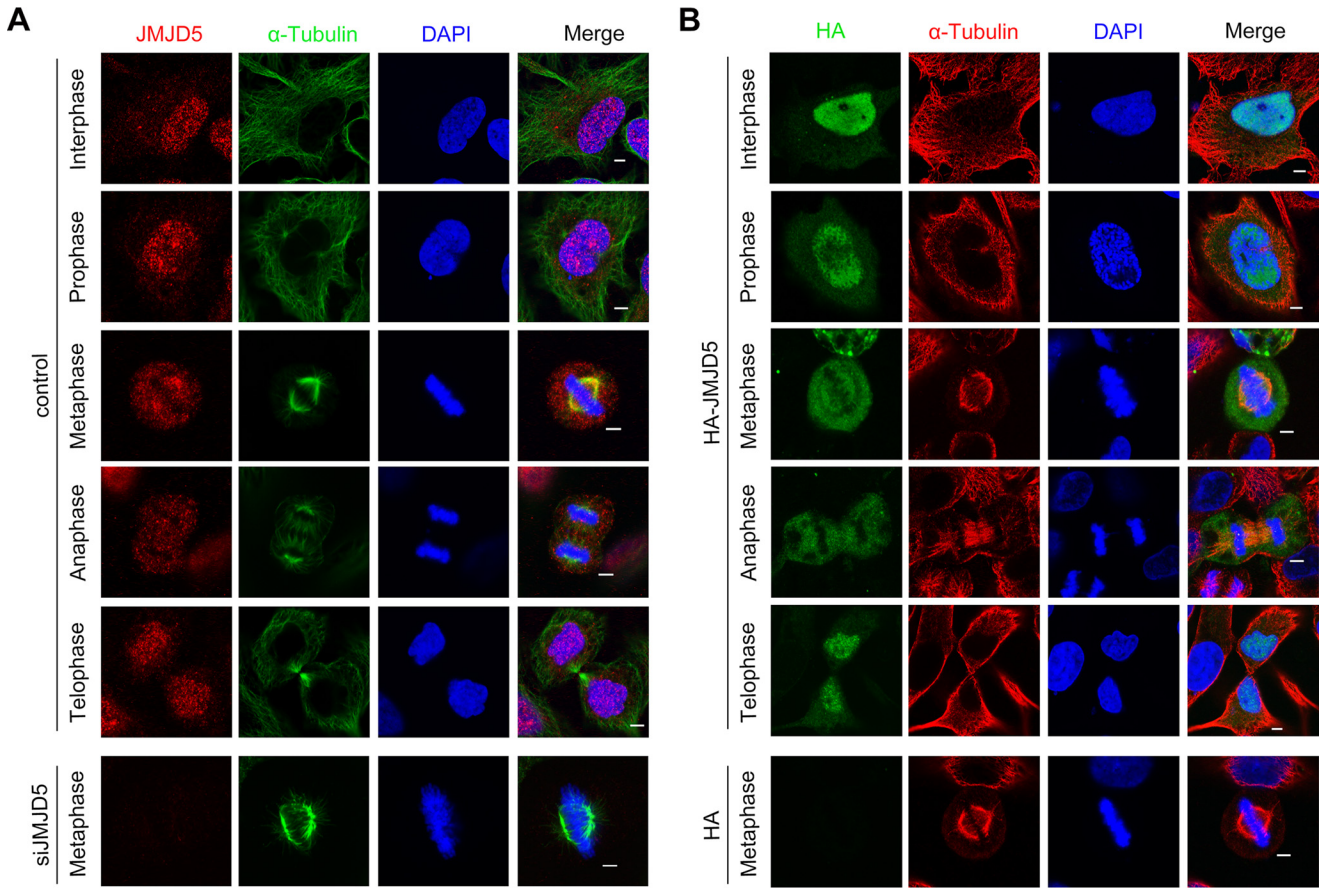

FIGURE 1. **JMJD5 partially localizes on mitotic spindles.** *A*, IF staining of control HeLa cells and JMJD5 knockdown cells with JMJD5 (*red*) and α-tubulin (*green*). *Blue*, DAPI. *B*, HeLa cells transfected with JMJD5-HA or HA control were stained with HA (*green*) and α-tubulin (*red*). *Blue*, DAPI. *Scale bars*, 5 μm.

were washed three times, and the associated proteins were eluted by GSH. The samples were then subjected to Western blot analysis.

Microtubule Co-sedimentation Assay—Microtubule co-sedimentation assay with cell lysate was performed as described previously with some modifications (26). In brief, HeLa cells were synchronized with 100 ng/ml nocodazole for 17 h and lysed in C buffer with complete protease inhibitor mixture (Roche) on ice for 30 min. Then the cell lysate was clarified by centrifugation and ultracentrifugation (Beckman Optima MAX-XP), and DTT and GTP (Thermo) were added to a final concentration of 1 mM. The mixture was incubated in water bath at 30 °C for 5 min and divided into two equal with volumes: one was placed on ice in the absence of taxol, and the other was placed in 37 °C water bath with taxol at a final concentration of 20 μM for 15 min. The samples were layered on top of cushion buffer and centrifuged at 100,000 × *g* for 40 min at 25 °C. The supernatant fractions and pellets were collected individually, and the distribution of proteins in each fraction was examined by immunoblotting.

Microtubule co-sedimentation assay with purified JMJD5 protein was performed using the kit from Cytoskeleton, Inc., according to the manufacturer's instructions. In brief, JMJD5-GST protein was dialyzed in general buffer prior to the assay. Purified tubulin proteins were incubated in general buffer with GTP at 35 °C for 20 min, and taxol was then added to stabilize the microtubules. Then the dialyzed JMJD5-GST was incubated alone or with different concentrations of microtubules (1–20 μM) in general buffer at 25 °C for 30 min. Samples were placed onto a 100-μl cushion buffer and centrifuged at 100,000 × *g* in a TLA100 rotor for 40 min at 25 °C. The pellets and supernatants were collected, suspended in sample buffer, and analyzed by Coomassie Blue staining or immunoblotting with anti-GST antibody.

Measurement of Interkinetochore Distance—HeLa cells transfected with siRNAs were seeded on polylysine-coated glass coverslips and then synchronized by DTB. 9 h after the second thymidine release, these cells were treated with 10 μM MG132 for 2 h. Then cells were fixed, and immunofluorescence assay was performed. Deconvolution images were collected and analyzed with Delta Vision Elite System (GE Healthcare) under 100× oil objective, and optical sections were taken at intervals of 0.2 μm. Distances were measured between sister kinetochores that were in the same confocal plane.

Results

JMJD5 Partially Localizes on Mitotic Spindles—To elucidate the role of JMJD5 in the cell cycle, we first investigated the expression changes of JMJD5 across the cell cycle. HeLa cells synchronized at the G_1/S boundary by DTB were released back into cell cycle. The expression level of JMJD5 slightly increased in the G_2-M phase (data no shown). Further, we investigated the localization of JMJD5 during cell cycle progression. We performed the immunofluorescent (IF) staining experiments in

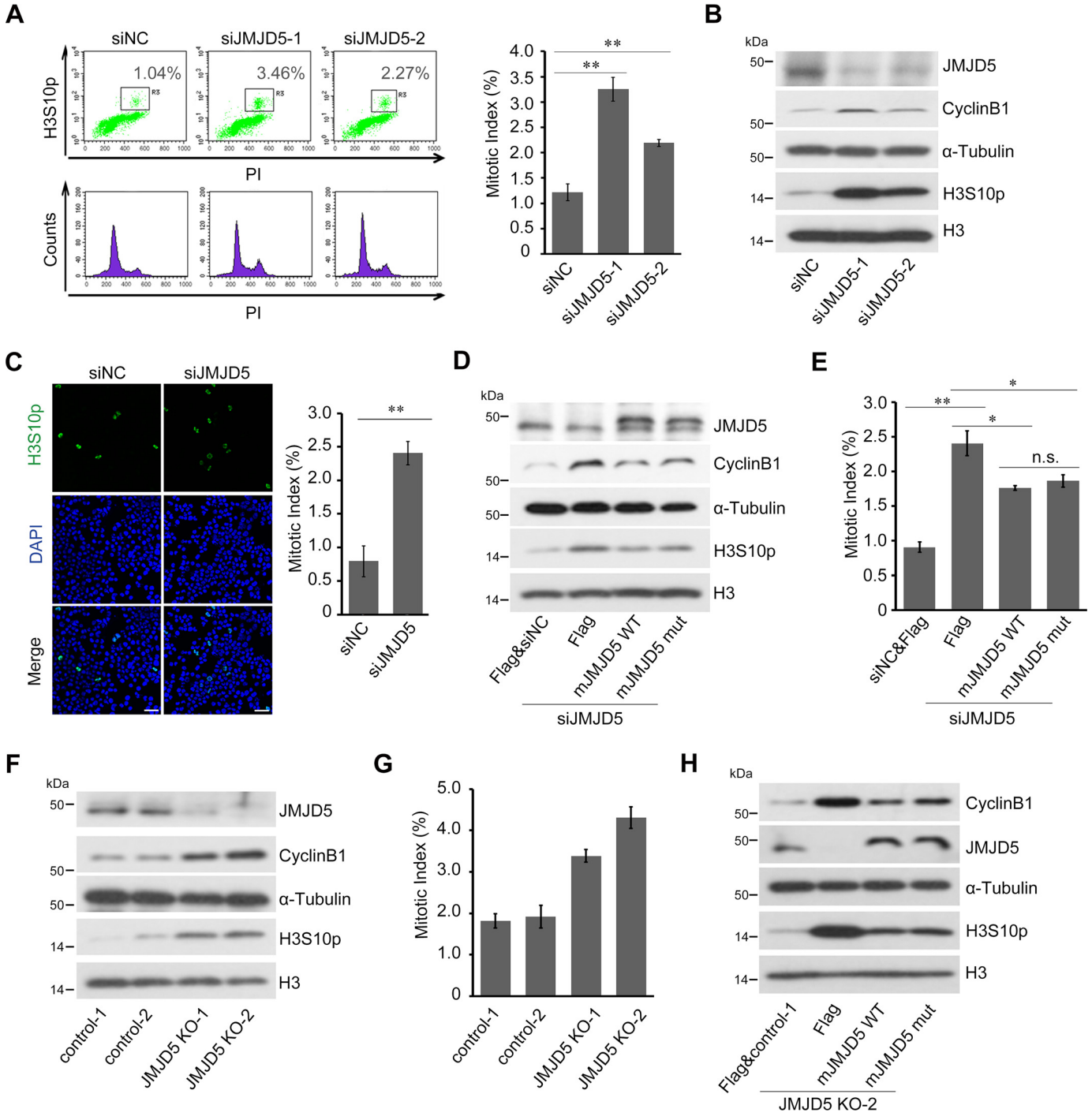

FIGURE 2. **Depletion of JMJD5 leads to significant mitotic cell accumulation.** *A*, the mitotic index increased in JMJD5-depleted cells. The cell cycle and mitotic index of indicated siRNAs transfected HeLa cells were analyzed by FACS using propidium iodide (*PI*) and an Alexa Fluor® 488 conjugate anti-phosphohistone H3Ser10 antibody. *B*, JMJD5 depletion leads to the increased level of cyclin B1 and histone H3Ser10 phosphorylation, tested by Western blot. *C*, IF visualization of mitotic cells. HeLa cells were transfected with the indicated siRNAs and stained for histone H3Ser10 phosphorylation (*green*) and DAPI (*blue*). *Scale bars*, 50 μm. The percentage of histone H3Ser10 phosphorylation positive cells was calculated. Approximately 2500 cells were counted per sample in three independent experiments. *D* and *E*, both mouse JMJD5 and its catalytic site inactive mutant mJMJD5 mut (H319A,D321A) can partially rescue the JMJD5-depletion induced mitotic arrest. Flag-mJMJD5 WT, Flag-mJMJD5 mut (H319A,D321A), and Flag vector were separately transfected into JMJD5-depleted HeLa cells. Mitotic markers were analyzed by Western blot (*D*), and mitotic index was measured by FACS (*E*). *Error bars* indicate $\pm$ S.E. *, $p < 0.05$; **, $p < 0.01$; *n.s.*, not significant by Student's *t* test. *F* and *G*, CRISPR/Cas9-mediated JMJD5 knock-out also results in mitotic cell accumulation. JMJD5 knock-out cell lines were generated as described under "Experimental Procedures." The levels of mitotic markers were tested by Western blot (*F*), and mitotic index was measured by FACS (*G*). *H*, both wild-type and mutant mJMJD5 could partially rescue the mitotic arrest phenotype in JMJD5 knock-out cells. Control-1 and JMJD5 KO-2 cells were transfected with indicated plasmids. Mitotic markers were analyzed by Western blot with indicated antibodies.

HeLa cells transfected with control siRNA or siJMJD5. As shown in Fig. 1*A*, we observed that JMJD5 localized mainly in the nucleus during interphase and early prophase. Surprisingly, after the nuclear envelope breaking down, JMJD5 diffused into the cytoplasm, and some localized onto mitotic spindles, whereas little signals could be detected on chromosomes.

Meanwhile, little signals could be observed in JMJD5-depleted metaphase cells (Fig. 1*A*) and cells in other mitotic stages (data not shown), confirming the specificity of the antibody and the localization of JMJD5. To verify this localization, human JMJD5-HA fusion protein was overexpressed in HeLa cells, and its localization was detected using an anti-HA antibody (Fig. 1*B*). Consistent with the phenomenon detected with the endogenous antibody, JMJD5-HA signals also concentrated on mitotic spindles during mitosis. Once the nuclear envelope reformed, JMJD5 was found to relocalize in the nucleus (Fig. 1, *A* and *B*). The localization of JMJD5 on mitotic spindles implies that JMJD5 may play a distinct role in cell mitotic progression.

Depletion of JMJD5 Leads to Accumulation of Mitotic Cells and Spindle Assembly Defects—The spindle apparatus ensures appropriate separation of chromosomes into daughter cells during mitosis. To investigate the function of JMJD5 in mitotic progression, we next examined the effects of JMJD5 depletion on mitosis using two distinct siRNAs against JMJD5. FACS analysis was performed to detect the mitotic index and DNA content at the same time. As shown in Fig. 2*A*, a G_2/M arrest in JMJD5-depleted cells was observed, consistent with previous report (13). Notably, a significant increase in the mitotic index was observed in JMJD5 knockdown cells as well (Fig. 2*A*). To verify this mitotic index increase, we performed Western bolt of mitotic markers and cell counts after IF staining assays. Consistently, JMJD5 depletion up-regulated the level of histone H3Ser10 phosphorylation and cyclin B1, two mitotic markers (Fig. 2*B*), and increased the number of phosho-H3Ser10 positive cells in IF assay (Fig. 2*C*).

JMJD5 is highly conserved in evolution. Orthologs of JMJD5 in human (hJMJD5) and mouse (mJMJD5) share 77% amino acid identity. In particular, the identity of the JmjC domain is as high as 90%. Further, Flag-tagged mJMJD5 showed same localization pattern in HeLa cells as hJMJD5 did (data not shown). To further validate the result that JMJD5 depletion was responsible for the elevation of the mitotic index, mJMJD5 was reintroduced into JMJD5-depleted HeLa cells. As shown in Fig. 2 (*D* and *E*), the increase of mitotic markers and the mitotic index caused by JMJD5 depletion were partially reversed in cells overexpressing mJMJD5. JMJD5 was reported to be histone H3K36me2 demethylase and non-histone protein hydroxylase (13, 16). The crystal structure of JMJD5 showed that, in the catalytic site, Fe^{2+} could be chelated by residues His^{321}, Asp^{323}, and His^{400} (27, 28). This H*X*(D/E)X_nH motif is highly conserved in JmjC domain-containing proteins and is important for their catalytic activity (29). To further investigate whether the enzymatic activity of JMJD5 is responsible for its function during mitosis, we designed the catalytically inactive mutant of mJMJD5 (H319A/D321A), which is related to H321A/D323A of hJMJD5. To our surprise, the mJMJD5 H319A/D321A mutant was also able to partially reverse the elevation of mitotic index caused by JMJD5 depletion similar to wild-type mJMJD5 (Fig. 2, *D* and *E*).

Because CRISPR/Cas9 mediate gene knock-out has now been widely used in gene functional test (30, 31), we also generated the CRISPR/Cas9 JMJD5 knock-out cell lines to examine the function of JMJD5 on mitosis. As shown in Fig. 2 (*F* and *G*), JMJD5 knock-out cell lines also showed higher levels of mitotic markers (Fig. 2*F*) and mitotic index (Fig. 2*G*) compared with control cell lines. Also, both wild-type and mutant mJMJD5 were able to partially rescue the mitotic arrest caused by JMJD5 knock-out (Fig. 2*H*). The results confirm that JMJD5 is required for proper mitosis, and this function may not dependent on the catalytic activity of JMJD5.

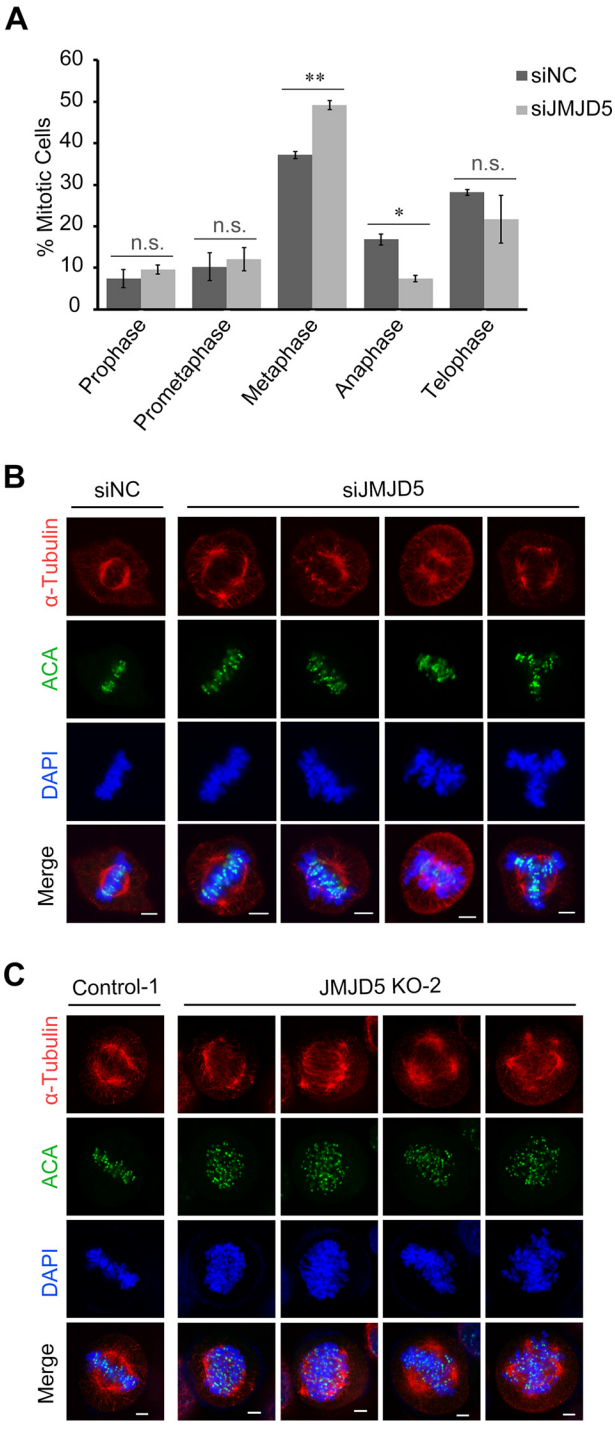

FIGURE 3. **Depletion of JMJD5 causes aberrant mitotic spindles.** HeLa cells were transfected with the indicated siRNAs. Immunofluorescent staining was performed with α-tubulin (*red*), ACA (*green*), and DAPI (*blue*). *Scale bars*, 5 μm. *A*, the stages of mitotic cells were distinguished according to chromatin morphology. $n = 119$ for siNC, and $n = 164$ for siJMJD5. *B* and *C*, different kinds of spindle defects were found in both JMJD5 knockdown cells (*B*) and JMJD5 knock-out cells (*C*).

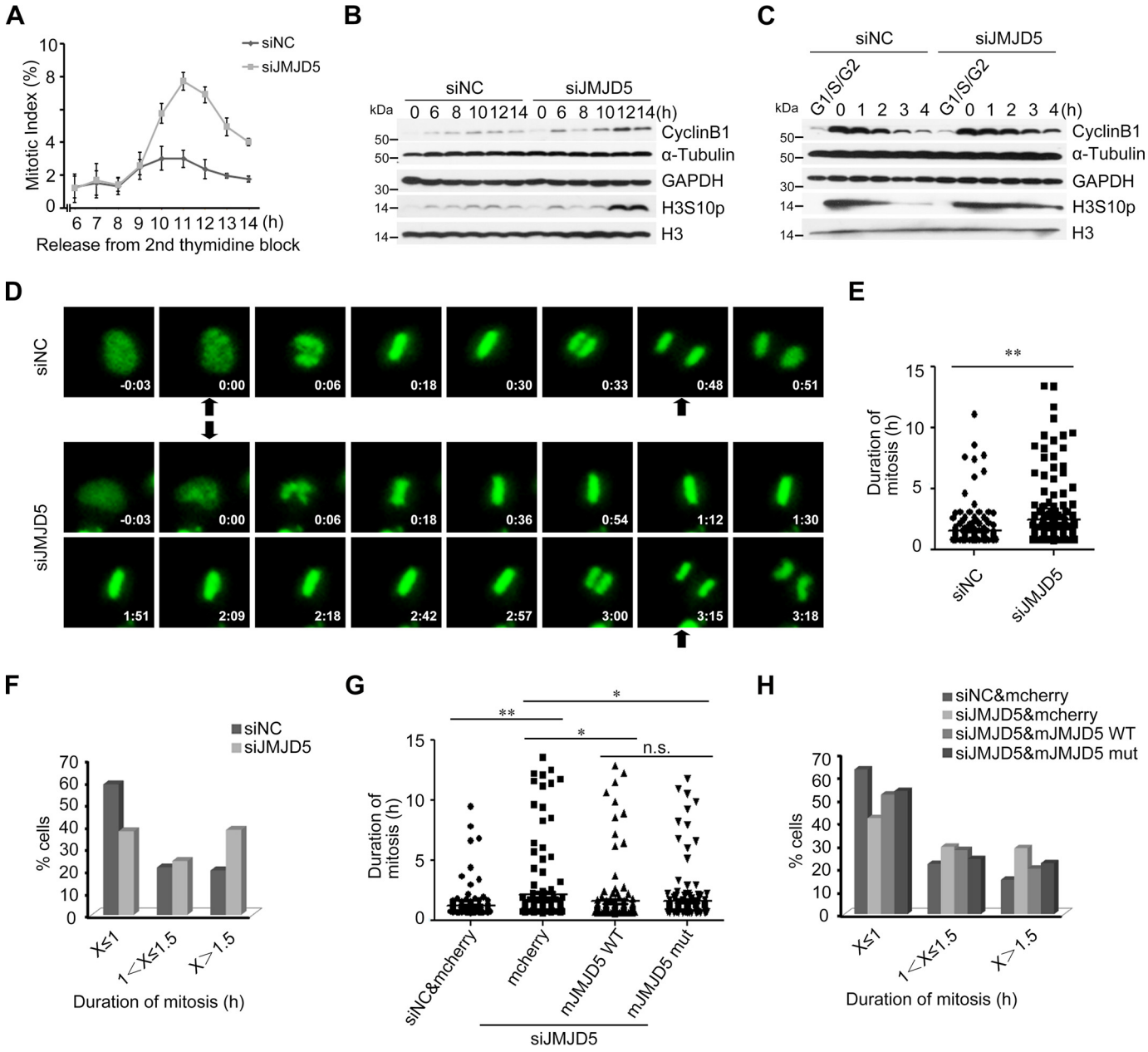

FIGURE 4. **Depletion of JMJD5 prolongs mitotic progression.** *A* and *B*, the effects of JMJD5 depletion on cell cycle progression after DTB synchronization. DTB-synchronized HeLa cells were released and collected at the indicated time points as showed. Mitotic index was measured by FACS (*A*), and mitotic markers were analyzed by Western blot (*B*). *C*, JMJD5 depletion delayed mitotic exit. Mitotic cells were harvested by shake-off after nocodazole treatment and released back into the cell cycle. The cells were collected at the indicated time points and analyzed by Western blot. *D–F*, JMJD5-depleted cells exhibited prolonged mitosis. Selected frames from time lapse microscopy of HeLa/H2B-GFP cells transfected with indicated siRNAs. *Black arrows* marked the start and end points of mitosis, with detailed description in "Experimental Procedures" (*D*). The duration of mitosis was measured (*E*) and categorized (*F*). $n = 150$ for siNC, and $n = 165$ for siJMJD5. *G*, prolonged mitotic progression can be partially reversed by both mouse JMJD5 and its catalytic site inactive mutant mJMJD5-mut. HeLa/H2B-GFP cells were transfected with JMJD5 siRNA together with indicated plasmids, and the duration of mitosis of mcherry positive cells were measured. $n = 160$ for siNC and mcherry, $n = 160$ for siJMJD5 and mcherry, $n = 159$ for siJMJD5 and mJMJD5-WT, and $n = 159$ for siJMJD5 and mJMJD5-mut. *H*, the duration of mitosis in the rescue assay was categorized, and a significant rescue effect was observed. *Error bars* indicate ± S.E. *, $p < 0.05$ by Student's *t* test.

Meanwhile, IF staining of α-tubulin and ACA was performed, and cells in different mitotic stages were counted according to chromatin morphology. As shown in Fig. 3*A*, knockdown of JMJD5 caused a significantly increased percentage in metaphase cells and a decreased percentage in anaphase cells among mitotic cells. Moreover, various patterns of abnormal mitotic spindles were observed in both JMJD5 knockdown cells (Fig. 3*B*) and JMJD5 knock-out cells (Fig. 3*C*). Taken together, these results suggest that JMJD5 plays an important role in regulating mitotic process and spindle assembly.

Depletion of JMJD5 Delays Mitotic Exit by Activating SAC—There are two possible causes for accumulation of mitotic cells. One is the shortening of premitotic processes (G_1 phase, S phase, or G_2 phase), and the other is the prolongation of mitosis. To precisely elucidate the phenomenon caused by JMJD5 depletion, we synchronized siRNA-transfected HeLa cells by

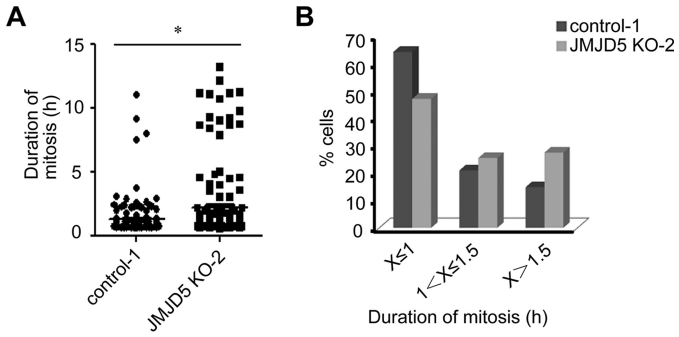

FIGURE 5. **JMJD5 knock-out prolongs mitotic progression.** Control-1 and JMJD5 KO-2 HeLa cell-lines were transfected with H2B-GFP plasmid, and time lapse microscopy imaging was performed. The duration of mitosis was measured (*A*) and categorized (*B*). $n = 162$ for control-1, and $n = 154$ for JMJD5 KO-2. *Error bars* indicate ± S.E. *, $p < 0.05$ by Student's *t* test.

DTB, and released these cells for different durations to analyze the mitotic index over time. As shown in Fig. 4*A*, the mitotic index curve of JMJD5-depleted cells showed no significant difference compared with the curve of control cells at mitotic entry (8 h after release), but it was higher at all times after that. Moreover, the height of the mitotic index curve of JMJD5-depleted cells was twice as high as that of control cells, and the former curve failed to decline to the basal level (level before mitotic entry) as observed for control cells. Consistent with the changes in the mitotic index, a marked increase and a delayed decline of the mitotic markers were also detected in JMJD5-depleted cells (Fig. 4*B*). These data suggest that JMJD5-depleted cells may obtain a prolonged mitotic phase. To further validate this possibility, we synchronized the siRNA-trans-

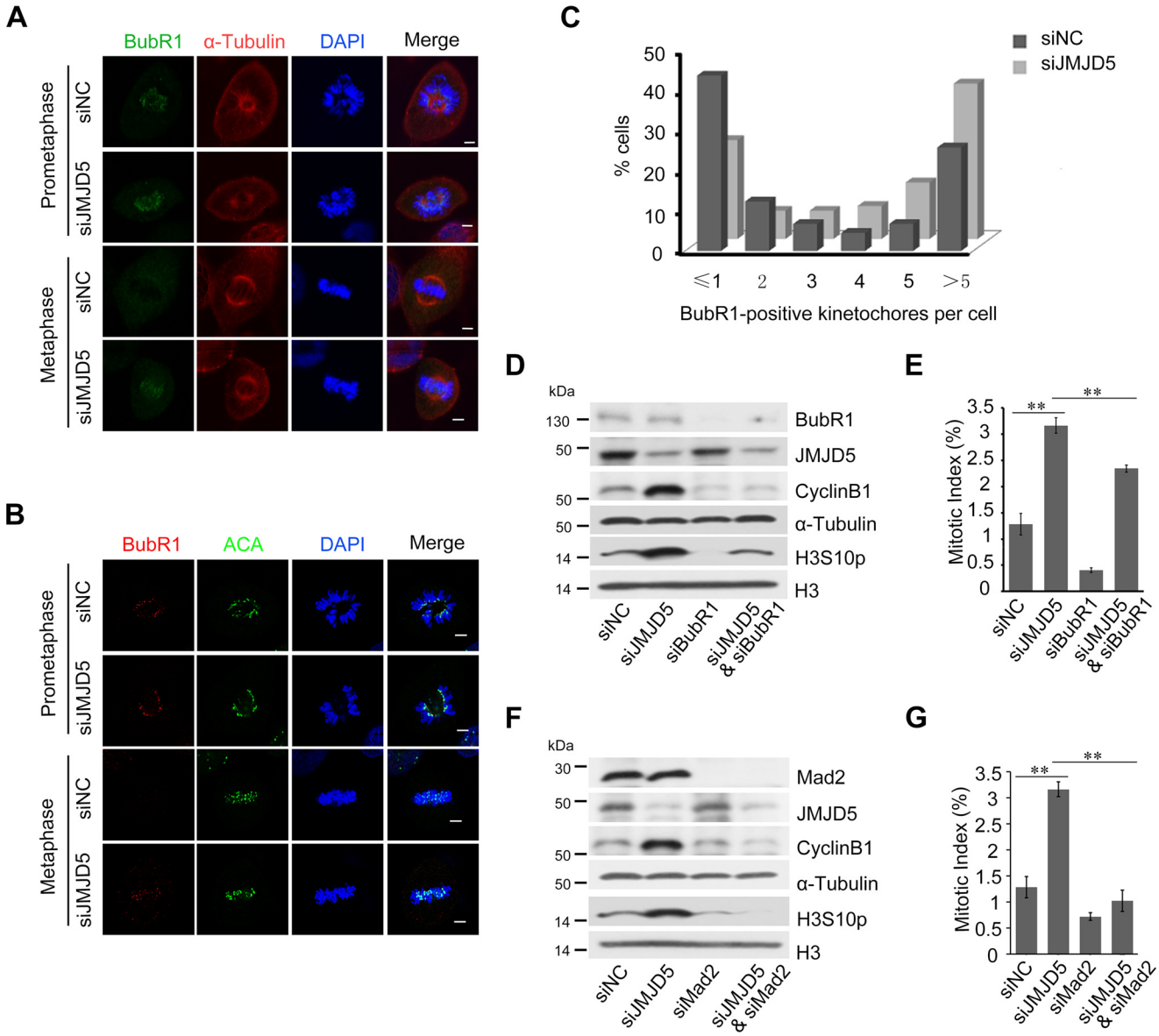

FIGURE 6. **Depletion of JMJD5 causes sustained SAC activation.** *A–C*, the effects of JMJD5 depletion on the recruitment of BubR1 to kinetochores. HeLa cells transfected with indicated siRNAs were synchronized by DTB and released for 10 h. Prometaphase and metaphase cells were stained with BubR1 (*green*) and α-tubulin (*red*) (*A*) or BubR1 (*red*) and ACA (*green*) (*B*), respectively. *Scale bars*, 5 μm. Cells with different number of BubR1 positive kinetochores were categorized (*C*). $n = 89$ for siNC), and $n = 85$ for siJMJD5. *D* and *E*, BubR1 knockdown can rescue JMJD5-depletion induced mitotic arrest. HeLa cells were transfected with the indicated siRNAs. Cell extracts were analyzed using Western blot with the indicated antibodies (*D*), and the mitotic index was measured by FACS (*E*). *F* and *G*, MAD2 knockdown can reverse JMJD5-depletion induced mitotic arrest. HeLa cells were transfected with the indicated siRNAs. Cell extracts were analyzed using Western blot with the indicated antibodies (*F*), and the mitotic index was measured by FACS (*G*). *Error bars* indicate ± S.E. **, $p < 0.01$ by Student's *t* test.

fected HeLa cells to the mitotic phase by "cell shake-off" after thymidine/nocodazole treatment and released them back into the cell cycle. As expected, JMJD5 knockdown cells showed a delayed decline of mitotic markers compared with control cells during mitotic progression (Fig. 4*C*). Taken together, these results indicate that JMJD5 plays an important role in regulating mitotic exit. To elucidate the mechanisms of mitotic delay induced by JMJD5 depletion, we next conducted time lapse microscopy of HeLa cells stably expressing histone H2B-GFP, with or without JMJD5 depletion. In control cells, most cells divided within 1 h with properly aligned chromosomes (Fig. 4, *D–F* and supplemental Movie S1). However, in JMJD5-depleted cells, the proper alignment of chromosomes was troubled and delayed, and cells stayed at metaphase for an extended time even after the unaligned chromosomes congressed. Nearly 40% of JMJD5-depleted cells needed more than 1.5 h to finish cell division, and some of them failed to separate or even died during this process (Fig. 4, *D–F* and supplemental Movie S2). Further, we reintroduced mJMJD5-WT-mcherry, mJMJD5-mut-mcherry fusion proteins, and mcherry into siRNA transfected HeLa/H2B-GFP cells. The duration of mitosis was analyzed in cells with red and green light. We found that, similar to the rescue of mitotic index, both wild-type and mutant mJMJD5 could partially rescue the prolonged mitosis caused by JMJD5 depletion (Fig. 4*G*), and the number of cells whose mitotic duration were longer than 1.5 h were significantly decreased after wild-type or mutant mJMJD5 transfection (Fig. 4*H*). Consistent with JMJD5 knockdown cells, JMJD5 knock-out cells also showed prolonged mitotic duration (Fig. 5, *A* and *B*).

The accumulation of metaphase cells and prolonged mitotic duration suggest that the SAC may be constantly activated in JMJD5-depleted cells. To verify this hypothesis, the association of BubR1 with kinetochores, a marker of SAC activation (5) was tested (Fig. 6, *A* and *B*). As expected, BubR1 was observed on kinetochores in both control cells and JMJD5 knockdown cells in prometaphase. In metaphase, BubR1 signals disappeared from the kinetochores in control cells, whereas it could still be detected at kinetochores in JMJD5 knockdown cells, even when the spindle was properly assembled (Fig. 6*A*) and the chromosomes were fully aligned (Fig. 6*B*). The number of BubR1 positive kinetochores was quantified (Fig. 6*C*), and the proportion of cells with more than 5 (>5) BubR1 positive kinetochores was significantly increased to 39% in JMJD5-depleted cells compared with control cells (25%). This indicated that more cells suffered a persistent SAC activation in JMJD5-depleted cells. To further confirm this, we depleted BubR1 or Mad2 to inactivate SAC (5, 6) in JMJD5-depleted cells, and then Western blot and FACS were performed to exam the mitotic changes. As shown in Fig. 6 (*D–G*), the accumulation of mitotic cells and the up-regulation of mitotic markers caused by JMJD5 knockdown could be reversed by further depletion of BubR1 or MAD2. Knock-out of JMJD5 also caused sustained activation of SAC (Fig. 7*A*), and the mitotic arrest could be rescued by additional knockdown of MAD2 (Fig. 7, *B* and *C*). Together, these results suggest that the mitotic arrest caused by JMJD5 depletion is in an SAC-dependent manner.

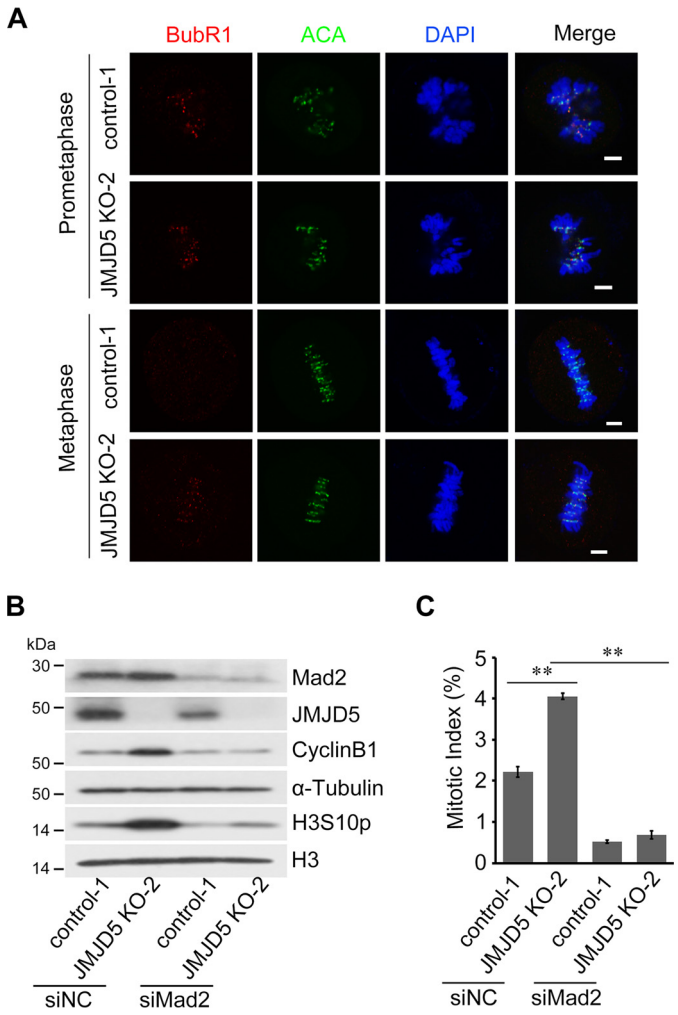

FIGURE 7. **Knock-out of JMJD5 causes mitotic arrest by SAC activation.** *A*, JMJD5 knock-out cells showed sustained activation of SAC in metaphase stage. Control-1 and JMJD5 KO-2 cells were stained with BubR1 (*red*) and ACA (*green*). *Scale bars*, 5 μm. Representative prometaphase and metaphase cells were shown. *B* and *C*, MAD2 knockdown can reverse JMJD5 knock-out-induced mitotic arrest. Control-1 and JMJD5 KO-2 cells were transfected with control siRNA or siRNA targeting MAD2. Mitotic markers were analyzed by Western blot (*B*), and mitotic index was measured by FACS (*C*).

Identification and Functional Assignment of the JMJD5-associated Proteins in Mitosis—To gain insight into how JMJD5 may regulate mitotic progression, we conducted MS to identify the protein partners of JMJD5 during the G_2/M phase. To this end, HeLa cells were transfected with C-terminal GFP-tagged hJMJD5 or GFP alone and synchronized by DTB. Then JMJD5 and its associated proteins were immunoprecipitated (IP) and analyzed by LC-MS/MS, as described in Fig. 8*A*. A total of 37 distinct JMJD5 interactors were identified (Table 1), and an interaction network of these interactors was generated using Cytoscape software according to the BioGRID database (Fig. 8*B*). A subset of these interactors was then confirmed by co-IP in nocodazole-synchronized HeLa cells (Fig. 8*D*) to validate the reliability of the MS assay. Moreover, the identified proteins were categorized into biological processes using a functional annotation tool, the Database for Annotation, Visualization and Integrated Discovery (DAVID), according to Gene Ontology annotations. A large portion of identified proteins were shown to be functionally implicated in cell cycle procession

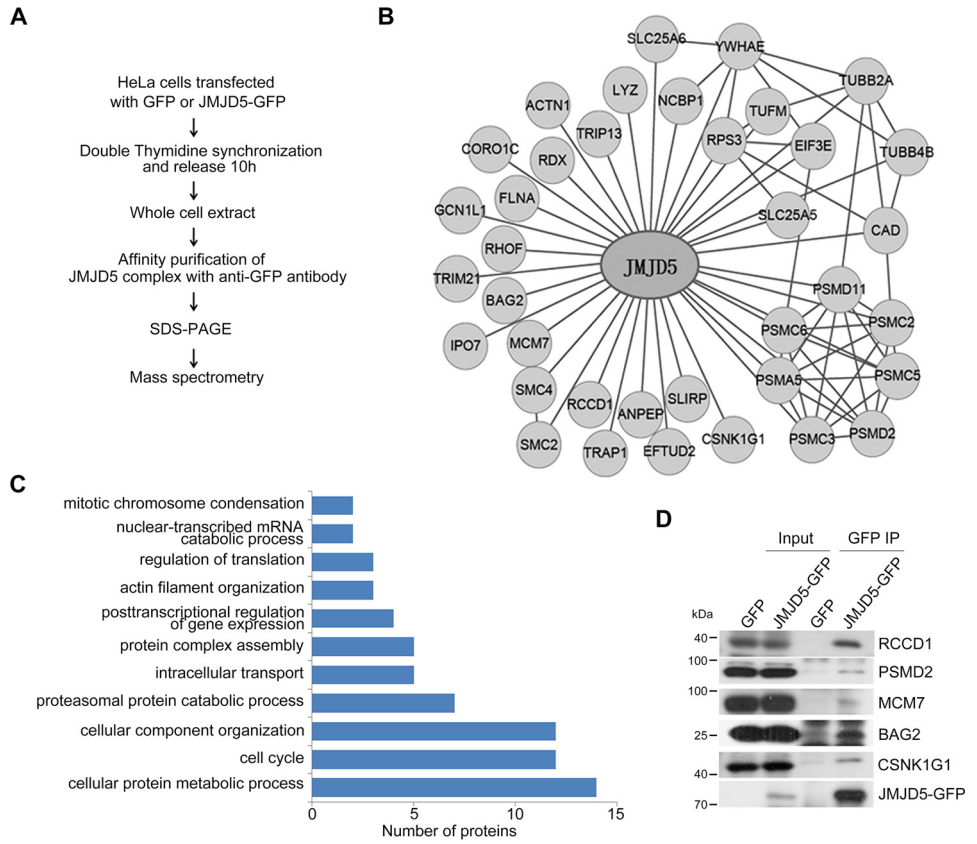

FIGURE 8. **Identification and functional assignment of the JMJD5 associated proteins in mitosis.** *A*, flow chart of steps to identify the interactors of JMJD5 during mitosis. *B*, the JMJD5 interaction network during mitosis identified by MS was assembled with Cytoscape. *C*, the identified proteins were categorized into biological process clusters of GO terms by DAVID functional annotation tool. *D*, co-immunoprecipitation was done to validate the interactions between JMJD5 and the selected interactors. Mitotic cell extracts were immunoprecipitated with anti-GFP antibody and analyzed using Western blot with indicated antibodies.

(Fig. 8*C*), indicating that JMJD5 might be involved in many ways in regulating cell cycle progression.

JMJD5 Interacts with Tubulin Proteins and Associates with Microtubules during Mitosis—Given the results that JMJD5 localized on spindles during mitosis (Fig. 1) and that tubulin proteins were identified in our MS assay (Table 1 and Fig. 8*B*), we proposed that JMJD5 may regulate mitotic progression by directly associating with microtubules. First, we confirmed the interaction between JMJD5 and tubulin proteins using co-IP in nocodazole-synchronized HeLa cells expressing GFP or the JMJD5-GFP fusion protein. Both α-tubulin and β-tubulin were co-precipitated with JMJD5 (Fig. 9*A*). Then we further examined whether JMJD5 directly interacted with tubulin proteins using GST pulldown assay. C-terminal GST-tagged JMJD5 was produced and purified from *E. coli*, and GST pulldown assays were performed with synchronized HeLa cell lysate. The result showed that α-tubulin and β-tubulin indeed bound to the JMJD5-GST fusion protein but not GST alone (Fig. 9*B*). These results indicate that JMJD5 interacts with tubulin proteins during mitosis.

To investigate whether JMJD5 could associate with polymerized tubulin (microtubules) during mitosis, we next performed microtubule co-sedimentation assay (26). Mitotic HeLa cells synchronized by nocodazole were lysed in specific buffer and pelleted by ultracentrifugation in the absence or presence of taxol. As shown in Fig. 9*C*, JMJD5 remained in the supernatant in the absence of taxol but partially presented in the pellet with tubulin proteins when taxol was added. To control the specificity, γ-tubulin, a known microtubule-associated protein, and MCM7, a JMJD5 interactor not associated with microtubules, were also examined (Fig. 9*C*). To further investigate whether JMJD5 could interact with microtubules in a cell-free system, JMJD5-GST protein was incubated alone or with varied concentrations of microtubules (1–20 μM), which were prepolymerized from purified tubulin proteins (cytoskeleton), and ultracentrifugation was performed. As shown in Fig. 9*D*, the binding of recombinant JMJD5 protein with microtubules was concentration-dependent and saturable. The percentage of JMJD5 in pellet fractions was quantified with ImageJ, and fitting analysis was carried out with GraphPad Prism (Fig. 9*E*). The binding constant of JMJD5 to microtubules is $\sim 2.23 \pm 0.7$ μM, indicating that the interaction of JMJD5 with microtubules was direct but with relatively low affinity. Taken together, these results indicate that JMJD5 could interact with tubulin proteins and associate with microtubules during mitosis.

JMJD5-depleted Cells Exhibit Low Acetyl-modified Spindles and Fail to Generate Enough Interkinetochore Tension—The above results indicate that JMJD5 may function as a novel microtubule-associated protein during mitosis. Because many microtubule-associated proteins are involved in the regulation of mitotic spindle dynamics (11, 12), we wondered whether the mitotic arrest and spindle defects induced by JMJD5 depletion

TABLE 1

JMJD5 interactors identified by mass spectrometry.

The number of identified unique peptides in the control sample is presented in parentheses.

Accession	Name	Sequence coverage	Unique peptides
		%	
IPI00296340	JMJD5	74.52	39 (0)
IPI00221224	ANPEP	34.23	34 (24)
IPI00018971	TRIM21	60.42	29 (23)
IPI00007752	TUBB4B	69.66	23 (18)
IPI00399158	RCCD1	63.83	20 (0)
IPI00943173	CORO1C	40.93	19 (7)
IPI00013475	TUBB2A	48.99	18 (15)
IPI00011253	RPS3	55.97	15 (10)
IPI00021435	PSMC2	29.56	11 (4)
IPI00000643	BAG2	31.28	8 (0)
IPI00979423	PSMC3	28.21	8 (3)
IPI00003505	TRIP13	24.77	8 (4)
IPI01011340	ACTN1	11.56	8 (5)
IPI00291467	SLC25A6	28.86	7 (4)
IPI00105598	PSMD11	22.22	7 (4)
IPI00007188	SLC25A5	23.15	7 (4)
IPI00646055	TRAP1	12.6	6 (3)
IPI00553169	FLNA	3.59	6 (2)
IPI00893035	CAD	3.05	6 (0)
IPI00555749	PSMC5	19.13	5 (2)
IPI00926410	PSMD2	6.94	4 (0)
IPI01013150	CSNK1G1	8.2	3 (0)
IPI01009289	RDX	5.59	3 (0)
IPI00007402	IPO7	4.24	3 (0)
IPI00328298	SMC4	2.6	3 (0)
IPI00001159	GCN1L1	1.46	3 (0)
IPI00019038	LYZ	27.03	2 (0)
IPI00009922	SLIRP	22.02	2 (0)
IPI00974080	EIF3E	14.6	2 (0)
IPI00307458	RHOF	9.48	2 (0)
IPI00291922	PSMA5	9.13	2 (0)
IPI00974544	YWHAE	8.15	2 (0)
IPI00926977	PSMC6	7.2	2 (0)
IPI00027107	TUFM	6.81	2 (0)
IPI01010977	SMC2	6.47	2 (0)
IPI00376143	MCM7	6.26	2 (0)
IPI00917777	EFTUD2	2.35	2 (0)
IPI00019380	NCBP1	4.18	2 (0)

were resulted from disturbed spindle stability. We examined the level of acetylated α-tubulin, an indicator of stable and long-lived microtubules (32), in siRNA-transfected HeLa cells. As shown in Fig. 10*A*, knockdown of JMJD5 significantly reduced the level of acetyl-α-tubulin. Notably, a marked decrease of acetylated α-tubulin was observed on mitotic spindles (Fig. 10*B*). JMJD5 knock-out cells also showed reduced level of acetyl-α-tubulin (Fig. 10*C*). Consistent with the impact of JMJD5 on mitotic arrest (Fig. 2*D*), this reduction of acetyl-α-tubulin was at least partially reversed by the overexpression of mJMJD5 or the mJMJD5 H319A/D321A mutant (Fig. 10*D*), indicating that this regulation may also occur independent of its enzymatic activity. Meanwhile, taxol, a microtubule-stabilizing reagent, could partially reverse this reduction of acetylated α-tubulin (Fig. 10*E*). To further investigate the relationship between mitotic arrest and the destabilization of spindles, both caused by JMJD5 depletion, we treated siRNA transfected cells with tubastatin A, a specific HDAC6 inhibitor (33). As shown in Fig. 10*F*, after the treatment of tubastatin A, the level of acetyl-α-tubulin showed a significant reverse, and the mitotic arrest (marked by H3Ser10 phosphorylation level) was also partially rescued. This result further demonstrates that JMJD5 is needed for proper mitosis at least in part through modulating the stability of spindle microtubules.

The stability and dynamics of spindle is important to generate enough interkinetochore tension to satisfy SAC (5, 6). To evaluate the effects of JMJD5 depletion on the interkinetochore tension, we measured the distance between sister kinetochores (34, 35). As shown in Fig. 10*G*, the distance between sister kinetochores of metaphase cells was shorter in JMJD5-depleted cells (1.176 ± 0.0217 μm) than that in control cells (1.439 ± 0.0344 μm), indicating a lack of tension between paired kinetochores. Thus, depletion of JMJD5 reduced the stability of spindle microtubules and abolished the tension across paired kinetochores, resulting in sustained SAC activation and mitotic delay.

The dynamics of spindle microtubules is one of the most successful targets of anti-cancer therapy (36). We wondered whether depletion of JMJD5 could alter the sensitivity of cancer cells to antimicrotubule agents. To verify this, HeLa cells transfected with JMJD5 or control siRNAs were treated with increasing concentrations of nocodazole and analyzed for cell viability with a Cell Counting Kit-8 (Beyotime). As shown in Fig. 10*H*, when treated with different concentrations of nocodazole, JMJD5-depleted cells showed much lower survival rate than control cells, indicating that they were more susceptible to nocodazole. Taken together, these results suggest that JMJD5 is essential for maintaining spindle microtubule stability, which is responsible for proper mitotic spindle function.

Discussion

Most of the previous studies of JMJD5 have focused on its role in gene transcriptional regulation in the nucleus. Here we report that JMJD5 plays an important role in mitotic progression. During mitosis, JMJD5 partially localizes on mitotic spindles. MS assay and biochemical analysis further demonstrate that JMJD5 could bind with tubulin proteins and associate with microtubules. Depletion of JMJD5 significantly reduces the level of acetyl-α-tubulin on mitotic spindles, which indicates that fewer stable spindle microtubules are assembled. This leads to abnormal spindle formation and fails to generate enough interkinetochore tension to satisfy the SAC. Finally, these defects result in mitotic arrest.

A large proportion of proteins have been found to show cell cycle-dependent localization changes (37). Recently, more and more epigenetic regulating proteins, which mainly localize in the nucleus in interphase, have been reported to obtain new localizations and functions during mitosis. Some typical examples are that HDAC3 localizes on the spindles and affects spindle assembly (38); MeCP2 co-localizes with centrosomes and spindles, and its loss disturbs spindle morphology and mitosis (39); and WDR5 shows localization on the midbody during cytokinesis and regulates this process (40). In our study, immunostaining showed that JMJD5 also changed its localization during mitosis. It associated with mitotic spindles after nuclear envelope breaking down (Fig. 1). Indeed, a later experiment demonstrated that JMJD5 associated with microtubules during mitosis (Fig. 9). Little JMJD5 signal could be detected on chromosomes during mitosis (Fig. 1). This may be the result of chromatin condensation changes in this stage, or some kinds of mitotic specific modifications might happen on JMJD5. Once the nuclear envelope was reconstituted, JMJD5 was transported

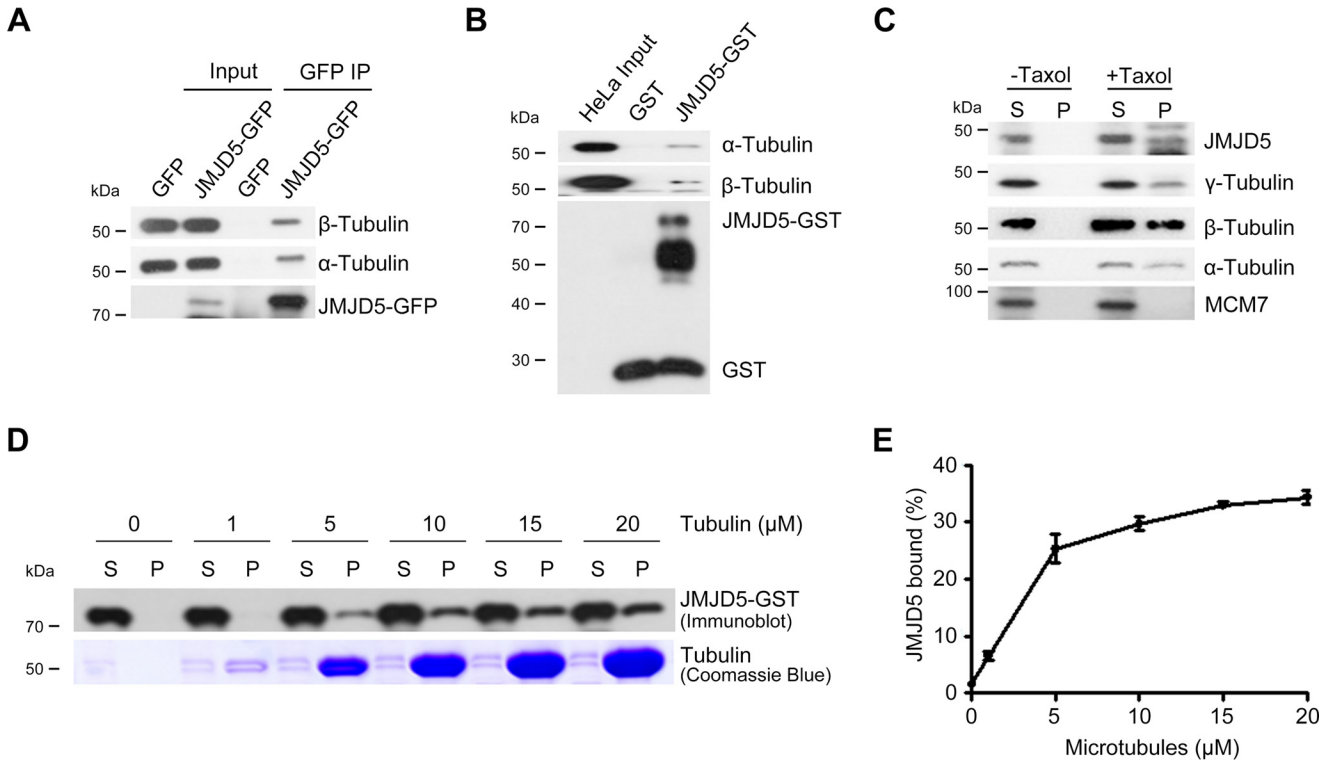

FIGURE 9. **JMJD5 interacts with tubulin proteins and associates with microtubules in mitotic cells.** *A*, HeLa cells transfected with the indicated plasmids were synchronized into mitosis by nocodazole. Anti-GFP immunoprecipitates (*IP*) were probed with the indicated antibodies. *B*, GST pulldown assay was performed with bacterially expressed GST or JMJD5-GST plus extracts of nocodazole-synchronized HeLa cells. The presence of tubulin proteins in the pulldown fraction were detected by Western blot. *C*, JMJD5 associated with microtubules during mitosis. Mitotic synchronization and microtubule co-sedimentation assay were performed as described under "Experimental Procedures." After ultracentrifugation in the absence or presence of taxol, proteins present in the pellet (*P*) and supernatant (*S*) fractions were detected by Western blot with the indicated antibodies. *D*, JMJD5 shows a direct interaction with microtubules *in vitro*. Purified JMJD5-GST protein was incubated alone or with varied concentrations of microtubules (1–20 μM), and ultracentrifugation was performed. JMJD5 in the pellet (*P*) and supernatant (*S*) fractions was detected by Western blot, and tubulin proteins were presented by Coomassie Blue staining. *E*, the percentage of JMJD5 that bound to microtubules (pellet fraction) was measured by densitometric analysis with ImageJ software.

back into the nucleus. This process may require a nuclear import system. In agreement with this hypothesis, a functional nuclear localization signal of JMJD5 has been reported, and importin α/β has been found to be associated with JMJD5 (41). Here, we also identified importin 7, which performed its nuclear import function by forming a heterodimer with importin β (42), as a JMJD5-associated protein by MS assay (Table 1 and Fig. 8*B*).

JMJD5 has been reported to be required for the cell cycle progression through transcriptional regulation of related genes, such as cyclin A1 (13) and Cdkn1a (14, 19). These functions are thought to be related to its histone H3K36me2 demethylase activity. To verify the influence of JMJD5 demethylase activity in its mitotic regulation, we designed the JmjC-inactive mutant (mJMJD5-H319A/D321A) for functional rescue of the phenotypes in JMJD5-depleted cells. Both wild-type and mutant mJMJD5 could partially reverse the destabilization of microtubules (Fig. 10*D*) and the mitotic arrest (Fig. 2, *D* and *H*) caused by JMJD5 depletion. Thus, the effects of JMJD5 on mitosis likely rely on a noncatalytic activity of JMJD5. Coincidentally, a recent report by Huang *et al.* (43) shows that the enzymatic activity of JMJD5 is not required for its cell cycle regulation in A549 cells. However, we have found that mutant JMJD5 also mostly located in the nucleus in interphase cells (data not shown). We could not exclude the possibility that the effects of JMJD5 on mitosis might also be through some indirect mechanisms involving the expression of cell cycle regulating genes or some signaling processes.

Spindle microtubule dynamics are important for chromosome alignment and mitotic progression (44). In this study, we revealed that JMJD5 could bind to tubulin proteins and associate with microtubules during mitosis. Purified JMJD5 showed a relatively low binding affinity to microtubules in *in vitro* microtubule co-sedimentation assay (Fig. 9*D*). The reason may be that some modifications acquired during mitosis do not exist in recombinant JMJD5 or because JMJD5 needs partners to elevate its binding affinity, like some other previously reported proteins. For example, CENP-E significantly enhances the binding affinity of SKAP to microtubules (45).

JMJD5 depletion significantly reduced the level of acetyl-α-tubulin on mitotic spindles (Fig. 10*B*). Furthermore, tubastatin A, a specific HDAC6 inhibitor, can significantly reverse the level of acetyl-α-tubulin and partially rescue the mitotic arrest caused by JMJD5 depletion (Fig. 10*F*). Thus, we speculate that modulating the stability of microtubules may be one of the main reasons for the important role of JMJD5 in proper mitosis. However, we failed to detect the interactions between JMJD5 and the reported tubulin acetyltransferases (ATAT1, ELP3, NAT1, NAT10, and GCN5) or tubulin deacetylases (HDAC6 and SIRT2) (9). Also, no significant differences in the protein level of these enzymes were found after knockdown of JMJD5 (data not shown). Thus, the regulation of tubulin acetylation

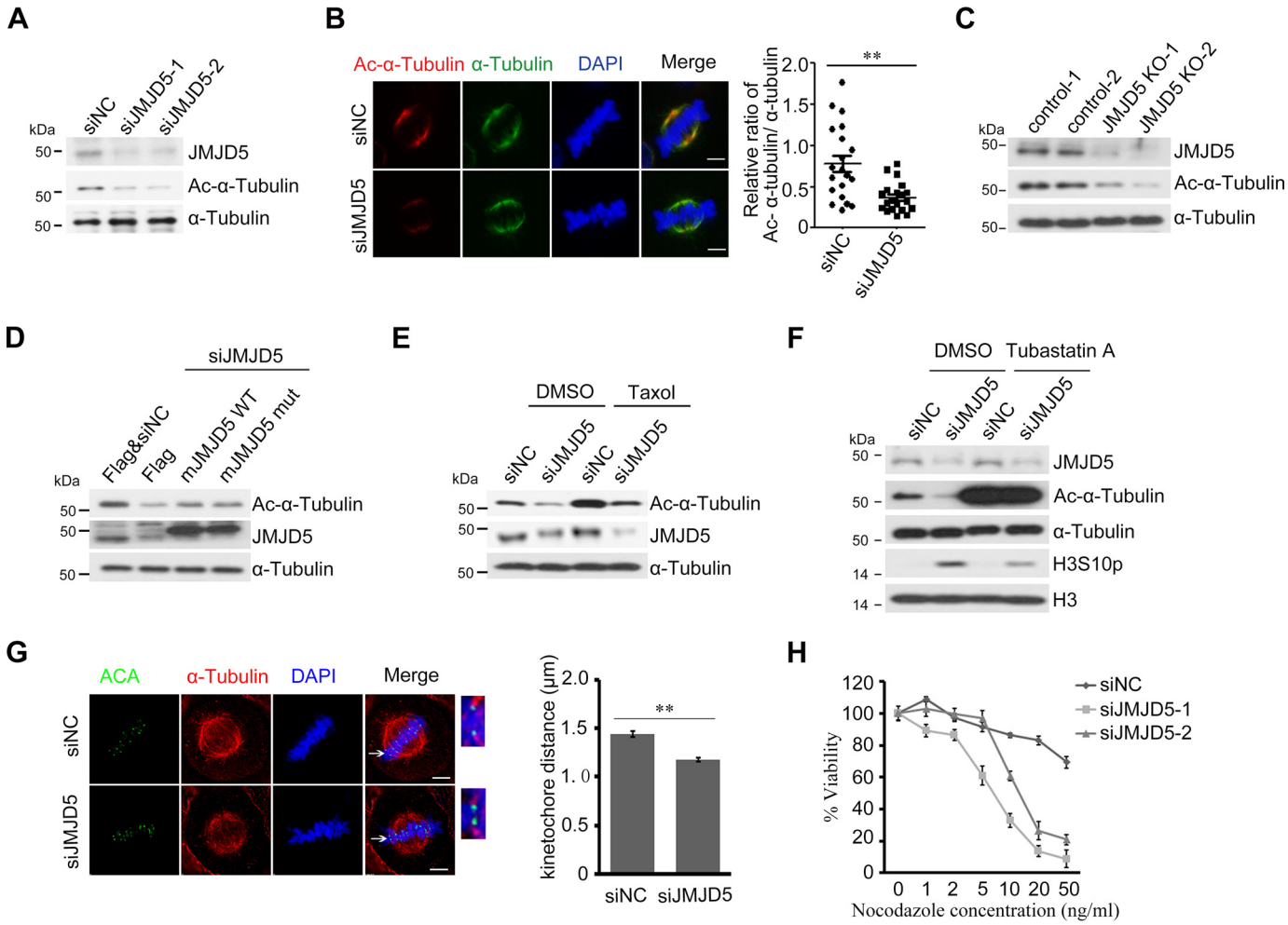

FIGURE 10. **JMJD5-depleted cells exhibit low acetyl-modified spindles and fail to generate enough interkinetochore tension.** *A*, knockdown of JMJD5 reduced the acetylation level of α-tubulin. HeLa cells were transfected with indicated siRNAs, and α-tubulin acetylation was measured by Western blot. *B*, IF analysis of acetylated α-tubulin in metaphase cells (*left panel*). The cells were stained for ac-α-tubulin (*red*) and α-tubulin (*green*). *Blue*, DAPI. *Scale bars*, 5 μm. The fluorescence intensities of ac-α-tubulin and α-tubulin were quantified by NIS-Elements software, and the ratio of ac-α-tubulin to α-tubulin was generated (*right panel*). $n = 20$ for siNC, and $n = 20$ for siJMJD5. *Error bars* indicate ± S.E. **, $p < 0.01$ by Student's *t* test. *C*, knock-out of JMJD5 reduced the acetylation level of α-tubulin. The acetylation level of α-tubulin in control and JMJD5 knock-out cell lines was measured by Western blot (related to Fig. 2*F*). *D*, both mouse JMJD5 and its catalytically inactive mutant mJMJD5 mut (H319A,D321A) can partially rescue the JMJD5-depletion induced microtubule instability. Flag-mJMJD5 WT, Flag-mJMJD5 mut (H319A,D321A), and Flag vector were separately transfected into JMJD5-depleted HeLa cells. Acetylation level of α-tubulin was measured by Western blot. *E*, the destabilization of microtubules caused by JMJD5 depletion was partially rescued by taxol. The indicated siRNA-transfected cells were treated with DMSO or 10 nM taxol for 2 h, and α-tubulin acetylation was measured by Western blot. *F*, tubastatin A treatment can partially rescue the mitotic arrest caused by JMJD5 depletion. HeLa cells were treated with 5 μM tubastatin A or DMSO for 48 h after transfection with siRNAs. Samples were collected and measured by Western blot. *G*, interkinetochore tension decreased in JMJD5-depleted cells. HeLa cells transfected with specific siRNAs were synchronized and released, followed by MG132 treatment for 2 h. The cells were stained with ACA (*green*), α-tubulin (*red*), and DAPI (*blue*) (*left panel*). *Scale bars*, 5 μm. *White arrows* point to the enlarged kinetochores. The distances between interkinetochores in JMJD5 knockdown cells ($n = 126$) and control cells ($n = 127$) were quantified (*right panel*). *Error bars* indicate ± S.E. **, $p < 0.01$ by Student's *t* test. *H*, JMJD5 depletion significantly increased cell susceptibility to the antimicrotubule agent nocodazole. HeLa cells were transfected with indicated siRNAs, and cell viability was measured with a Cell Counting Kit-8 kit after treatment with various concentrations of nocodazole for 36 h.

and microtubule stability by JMJD5 seems not through directly recruiting or inhibiting acetylation-related enzymes. Therefore, the exact mechanisms of microtubule stability regulation by JMJD5 should be further studied in the future.

MS assay revealed protein complexes of JMJD5 in the G_2/M phase. A dozen proteins, apart from tubulin proteins, identified in our MS assay are involved in the cell cycle regulation (Fig. 8*C*). Therefore, modulating the stability of microtubules may not be the only manner by which JMJD5 regulates cell mitotic progression. For instance, JMJD5 also interacts with several 26S proteasome components, such as PSMD2 (Fig. 8*D*). In anaphase of mitosis, when anaphase-promoting complex/cyclosome is activated, substrates such as cyclin B and securin are degraded by the proteasome, promoting the mitotic exit program (5). Further studies are needed to test whether JMJD5 could directly regulate the proteasome degradation of cyclin B and securin or whether these interactions only account for the degradation of JMJD5 itself.

Microtubule dynamics also plays important roles in cancer cell migration, invasion, and metastasis (46, 47). The reduction of acetyl-α-tubulin caused by JMJD5 depletion (Fig. 10) implied that JMJD5 may also play a role in the regulation of cytoskeleton dynamics. It will be interesting to further explore whether JMJD5 depletion can regulate these important biological processes. Moreover, microtubule stability is a very appealing target for anticancer chemotherapy (36), and JMJD5-depleted

cells were found to be much more susceptible to the antimicrotubule agent nocodazole (Fig. 10*H*). Our future studies will also be focused on the relationship between JMJD5 expression level and drug sensitivity in cancer cells.

Author Contributions—F.-L. S, Z. H., and J. W. designed research; Z. H., J. W., X. S., Y. Z., L. P., H. W., and Q. F. performed research; Z. H., J. W., X. S., H. L., D.-L. W., and F.-L. S. analyzed data; and Z. H., J. W., X. S., H. L., and F.-L. S wrote the paper.

Acknowledgments—We thank Prof. Zhijie Chang (Tsinghua University, Beijing, China) for great help on this manuscript and pEF-Neo-Flag and pcDNA3.1-HA vector and Prof. Chuanmao Zhang (Peking University, Beijing, China) for kindly offering the ACA. We thank Tsinghua University SLSTU-Nikon biological imaging center and Imaging Core Facility, Tsinghua University Branch of China National center for protein science, Beijing for help with microscopy facilities. We also thank Cell Biology Facility & Protein Chemistry Facility at Center of Biomedical Analysis (Tsinghua University, Beijing, China) for help with FACS and MS assay.

References

1. Kops, G. J., Weaver, B. A., and Cleveland, D. W. (2005) On the road to cancer: aneuploidy and the mitotic checkpoint. *Nat. Rev. Cancer* **5,** 773–785
2. Carter, S. L., Eklund, A. C., Kohane, I. S., Harris, L. N., and Szallasi, Z. (2006) A signature of chromosomal instability inferred from gene expression profiles predicts clinical outcome in multiple human cancers. *Nat. Genet.* **38,** 1043–1048
3. Mitelman, F., Johansson, B., and Mertens, F. (2007) The impact of translocations and gene fusions on cancer causation. *Nat. Rev. Cancer* **7,** 233–245
4. Gordon, D. J., Resio, B., and Pellman, D. (2012) Causes and consequences of aneuploidy in cancer. *Nat. Rev. Genet.* **13,** 189–203
5. Musacchio, A., Salmon, E. D. (2007) The spindle-assembly checkpoint in space and time. *Nat. Rev. Mol. Cell Biol.* **8,** 379–393
6. Foley, E. A., and Kapoor, T. M. (2013) Microtubule attachment and spindle assembly checkpoint signalling at the kinetochore. *Nat. Rev. Mol. Cell Biol.* **14,** 25–37
7. Sudakin, V., Chan, G. K. T., and Yen, T. J. (2001) Checkpoint inhibition of the APC/C in HeLa cells is mediated by a complex of BUBR1, BUB3, CDC20, and MAD2. *J. Cell Biol.* **154,** 925–936
8. Janke, C. (2014) The tubulin code: Molecular components, readout mechanisms, and functions. *J. Cell Biol.* **206,** 461–472
9. Janke, C., and Bulinski, J. C. (2011) Post-translational regulation of the microtubule cytoskeleton: mechanisms and functions. *Nat. Rev. Mol. Cell Biol.* **12,** 773–786
10. Gruss, O. J., Carazo-Salas, R. E., Schatz, C. A., Guarguaglini, G., Kast, J., Wilm, M., Le Bot, N., Vernos, I., Karsenti, E., and Mattaj, I. W. (2001) Ran induces spindle assembly by reversing the inhibitory effect of importin alpha on TPX2 activity. *Cell* **104,** 83–93
11. Koffa, M. D., Casanova, C. M., Santarella, R., Kocher, T., Wilm, M., and Mattaj, I. W. (2006) HURP is part of a ran-dependent complex involved in spindle formation. *Curr. Biol.* **16,** 743–754
12. Raemaekers, T., Ribbeck, K., Beaudouin, J., Annaert, W., Van Camp, M., Stockmans, I., Smets, N., Bouillon, R., Ellenberg, J., and Carmeliet, G. (2003) NuSAP, a novel microtubule-associated protein involved in mitotic spindle organization. *J. Cell Biol.* **162,** 1017–1029
13. Hsia, D. A., Tepper, C. G., Pochampalli, M. R., Hsia, E. Y. C., Izumiya, C., Huerta, S. B., Wright, M. E., Chen, H. W., Kung, H. J., and Izumiya, Y. (2010) KDM8, a H3K36me2 histone demethylase that acts in the cyclin A1 coding region to regulate cancer cell proliferation. *Proc. Natl. Acad. Sci. U.S.A.* **107,** 9671–9676
14. Ishimura, A., Minehata, K., Terashima, M., Kondoh, G., Hara, T., and Suzuki, T. (2012) Jmjd5, an H3K36me2 histone demethylase, modulates embryonic cell proliferation through the regulation of Cdkn1a expression. *Development* **139,** 749–759
15. Oh, S., and Janknecht, R. (2012) Histone demethylase JMJD5 is essential for embryonic development. *Biochem. Biophys. Res. Commun.* **420,** 61–65
16. Youn, M. Y., Yokoyama, A., Fujiyama-Nakamura, S., Ohtake, F., Minehata, K., Yasuda, H., Suzuki, T., Kato, S., and Imai, Y. (2012) JMJD5, a Jumonji C (JmjC) Domain-containing Protein, Negatively Regulates Osteoclastogenesis by Facilitating NFATc1 Protein Degradation. *J. Biol. Chem.* **287,** 12994–13004
17. Wang, H. J., Hsieh, Y. J., Cheng, W. C., Lin, C. P., Lin, Y. S., Yang, S. F., Chen, C. C., Izumiya, Y., Yu, J. S., Kung, H. J., and Wang, W. C. (2014) JMJD5 regulates PKM2 nuclear translocation and reprograms HIF-1 alpha-mediated glucose metabolism. *Proc. Natl. Acad. Sci. U.S.A.* **111,** 279–284
18. Marcon, E., Ni, Z. Y., Pu, S. Y., Turinsky, A. L., Trimble, S. S., Olsen, J. B., Silverman-Gavrila, R., Silverman-Gavrila, L., Phanse, S., Guo, H. B., Zhong, G. Q., Guo, X. H., Young, P., Bailey, S., Roudeva, D., Zhao, D., Hewel, J., Li, J., Graslund, S., Paduch, M., Kossiakoff, A. A., Lupien, M., Emili, A., Wodak, S. J., and Greenblatt, J. (2014) Human-Chromatin-Related Protein Interactions Identify a Demethylase Complex Required for Chromosome Segregation. *Cell Reports* **8,** 297–310
19. Zhu, H., Hu, S. J., and Baker, J. (2014) JMJD5 Regulates Cell Cycle and Pluripotency in Human Embryonic Stem Cells. *Stem Cells* **32,** 2098–2110
20. Coulombe, P., and Meloche, S. (2002) Dual-tag prokaryotic vectors for enhanced expression of full-length recombinant proteins. *Anal. Biochem.* **310,** 219–222
21. Brownlow, N., Pike, T., Zicha, D., Collinson, L., and Parker, P. J. (2014) Mitotic catenation is monitored and resolved by a PKCepsilon-regulated pathway. *Nature communications* **5,** 5685
22. Juan, G., and Darzynkiewicz, Z. (2004) *Detection of mitotic cells.*, John Wiley & Sons
23. Huang, D. W., Sherman, B. T., and Lempicki, R. A. (2009) Systematic and integrative analysis of large gene lists using DAVID bioinformatics resources. *Nature Protocols* **4,** 44–57
24. Stark, C., Breitkreutz, B. J., Reguly, T., Boucher, L., Breitkreutz, A., and Tyers, M. (2006) BioGRID: a general repository for interaction datasets. *Nucleic Acids Res.* **34,** D535-D539
25. Saito, R., Smoot, M. E., Ono, K., Ruscheinski, J., Wang, P.-L., Lotia, S., Pico, A. R., Bader, G. D., and Ideker, T. (2012) A travel guide to Cytoscape plugins. *Nature Methods* **9,** 1069–1076
26. Antrobus, R., and Wakefield, J. G. (2011) Isolation, Identification, and Validation of Microtubule-Associated Proteins from Drosophila Embryos. in *Microtube Dynamics: Methods and Protocols*, Humana Press Inc, 999 Riverview Dr, Ste 208, Totowa, Nj 07512–1165 U.S.A. pp 273–291
27. Del Rizzo, P. A., Krishnan, S., and Trievel, R. C. (2012) Crystal Structure and Functional Analysis of JMJD5 Indicate an Alternate Specificity and Function. *Mol. Cell. Biol.* **32,** 4044–4052
28. Wang, H. P., Zhou, X., Wu, M. H., Wang, C. L., Zhang, X. Q., Tao, Y., Chen, N. N., and Zang, J. Y. (2013) Structure of the JmjC-domain-containing protein JMJD5. *Acta Crystallographica Section D-Biological Crystallography* **69,** 1911–1920
29. Klose, R. J., Kallin, E. M., and Zhang, Y. (2006) JmjC-domain-containing proteins and histone demethylation. *Nat. Rev. Genet.* **7,** 715–727
30. Cong, L., Ran, F. A., Cox, D., Lin, S. L., Barretto, R., Habib, N., Hsu, P. D., Wu, X. B., Jiang, W. Y., Marraffini, L. A., and Zhang, F. (2013) Multiplex Genome Engineering Using CRISPR/Cas Systems. *Science* **339,** 819–823
31. Mali, P., Yang, L. H., Esvelt, K. M., Aach, J., Guell, M., DiCarlo, J. E., Norville, J. E., and Church, G. M. (2013) RNA-Guided Human Genome Engineering via Cas9. *Science* **339,** 823–826
32. Szyk, A., Deaconescu, A. M., Spector, J., Goodman, B., Valenstein, M. L., Ziolkowska, N. E., Kormendi, V., Grigorieff, N., and Roll-Mecak, A. (2014) Molecular Basis for Age-Dependent Microtubule Acetylation by Tubulin Acetyltransferase. *Cell* **157,** 1405–1415
33. Butler, K. V., Kalin, J., Brochier, C., Vistoli, G., Langley, B., and Kozikowski, A. P. (2010) Rational Design and Simple Chemistry Yield a Superior, Neuroprotective HDAC6 Inhibitor, tubastatin A. *J. Am. Chem. Soc.* **132,** 10842–10846

34. Nicklas, R. B. (1997) How cells get the right chromosomes. *Science* **275,** 632–637
35. Rieder, C. L., and Salmon, E. D. (1998) The vertebrate cell kinetochore and its roles during mitosis. *Trends in Cell Biol.* **8,** 310–318
36. Jordan, M. A., and Wilson, L. (2004) Microtubules as a target for anticancer drugs. *Nat. Rev. Cancer* **4,** 253–265
37. Farkash-Amar, S., Eden, E., Cohen, A., Geva-Zatorsky, N., Cohen, L., Milo, R., Sigal, A., Danon, T., and Alon, U. (2012) Dynamic Proteomics of Human Protein Level and Localization across the Cell Cycle. *Plos One* **7**
38. Ishii, S., Kurasawa, Y., Wong, J. M., and Yu-Lee, L. Y. (2008) Histone deacetylase 3 localizes to the mitotic spindle and is required for kinetochore-microtubule attachment. *Proc. Natl. Acad. Sci. U.S.A.* **105,** 4179–4184
39. Bergo, A., Strollo, M., Gai, M., Barbiero, I., Stefanelli, G., Sertic, S., Gigli, C. C., Di Cunto, F., Kilstrup-Nielsen, C., and Landsberger, N. (2015) Methyl-CpG Binding Protein 2 (MeCP2) Localizes at the Centrosome and Is Required for Proper Mitotic Spindle Organization. *J. Biol. Chem.* **290,** 3223–3237
40. Bailey, J. K., Fields, A. T., Cheng, K. J., Lee, A., Wagenaar, E., Lagrois, R., Schmidt, B., Xia, B., and Ma, D. (2015) WD Repeat-containing Protein 5 (WDR5) Localizes to the Midbody and Regulates Abscission. *J. Biol. Chem.* **290,** 8987–9001
41. Huang, X. B., Zhang, L. N., Qi, H. Y., Shao, J. M., and Shen, J. (2013) Identification and functional implication of nuclear localization signals in the N-terminal domain of JMJD5. *Biochimie (Paris)* **95,** 2114–2122
42. Jaekel, S., Albig, W., Kutay, U., Bischoff, F. R., Schwamborn, K., Doenecke, D., and Goerlich, D. (1999) The importin beta/importin 7 heterodimer is a functional nuclear import receptor for histone H1. *EMBO (European Molecular Biology Organization) Journal* **18,** 2411–2423
43. Huang, X., Zhang, S., Qi, H., Wang, Z., Chen, H. W., Shao, J., and Shen, J. (2015) JMJD5 interacts with p53 and negatively regulates p53 function in control of cell cycle and proliferation. *Biochim. Biophys. Acta-Mol. Cell Res.* **1853,** 2286–2295
44. Wittmann, T., Hyman, A., and Desai, A. (2001) The spindle: a dynamic assembly of microtubules and motors. *Nat. Cell Biol.* **3,** E28-E34
45. Huang, Y. J., Wang, W. W., Yao, P., Wang, X. W., Liu, X., Zhuang, X. X., Yan, F., Zhou, J. H., Du, J., Ward, T., Zou, H. F., Zhang, J. C., Fang, G. W., Ding, X., Dou, Z., and Yao, X. B. (2012) CENP-E Kinesin Interacts with SKAP Protein to Orchestrate Accurate Chromosome Segregation in Mitosis. *J. Biol. Chem.* **287,** 1500–1509
46. Kaverina, I., and Straube, A. (2011) Regulation of cell migration by dynamic microtubules. *Seminars in Cell & Developmental Biology* **22,** 968–974
47. Castro-Castro, A., Janke, C., Montagnac, G., Paul-Gilloteaux, P., and Chavrier, P. (2012) ATAT1/MEC-17 acetyltransferase and HDAC6 deacetylase control a balance of acetylation of alpha-tubulin and cortactin and regulate MT1-MMP trafficking and breast tumor cell invasion. *European Journal of Cell Biol.* **91,** 950–960